Indoor Air 2009; 19: 324–334
www.blackwellpublishing.com/ina

INDOOR AIR
doi:10.1111/j.1600-0668.2009.00595.x

The influence of chemical interactions at the human surface on breathing zone levels of reactants and products

Abstract Using computational fluid dynamics simulations of an occupant in a ventilated room, we find that breathing zone ozone levels can be substantially lower and ozone reaction products associated with human surfaces (ORPHS) levels considerably higher than room levels. For air exchange rates < 3/h, the ratio of the breathing zone to the ozone concentration 1 m from the body (bulk air), r_{ozone}, ranges from 0.59 to 0.75 for floor or ceiling air supply. ORPHS are enriched in the breathing zone, with concentrations for these conditions ranging from 1.2 to 2.5 greater than bulk air concentrations. At high air exchange rates (> 8/h), the breathing zone concentrations approach bulk air concentrations ($r_{ozone} > 0.9$) with a floor supply, whereas large concentration gradients occur between breathing zone and bulk air with a ceiling supply. At these high air exchange rates, ORPHS levels are 1.6–2.0 and 2.9–6.0 times the bulk air concentrations for floor and ceiling supply, respectively. The extent of depletion of ozone or enrichment of ORPHS is large enough that reliance on micro-environmental measurements alone, to assess the intake of ozone or ORPHS, is undesirable.

D. Rim[1], A. Novoselec[1], G. Morrison[2]

[1]Department of Civil, Environmental and Architectural Engineering, University of Texas at Austin, Austin, TX, USA, [2]Department of Civil, Architectural and Environmental Engineering, Missouri University of Science and Technology, Rolla, MO, USA

Key words: Ozone; Human surface; Ozone reaction products; CFD; Exposure; Breathing zone concentration.

G. Morrison
Department of Civil, Architectural and Environmental Engineering
Missouri University of Science and Technology
Rolla, MO, USA
Tel.: (573) 341-7192
Fax: (573) 341-4729
e-mail: gcm@mst.edu

Received for review 17 November 2008. Accepted for publication 6 January 2009.

Practical Implications
Chemical reactions between ozone and human and clothing surfaces are predicted to significantly reduce ozone concentrations, and increase ozone reaction products associated with human surfaces (ORPHS) concentrations, in the breathing zone, relative to those concentrations in the larger microenvironment of a room. Existing measurements may overestimate ozone exposure and intake in typical indoor environments.

Introduction

Indoor micro-environmental concentrations of pollutants can differ by orders of magnitude relative to outdoor levels. In the absence of indoor sources, chemically reactive smog species, such as ozone, nitrogen dioxide and nitric acid, are usually present at lower levels because of reactions with or sorption to surfaces. Given that people spend most of their time in buildings (Klepeis et al., 2001), these differences make consideration of indoor contamination levels imperative when evaluating personal exposure to individual or classes of pollutants (Weschler et al., 1989). Just as important as the building environment is the personal microenvironment and especially a person's breathing zone. The term 'personal cloud' refers to the tendency for some pollutants, heretofore mainly particles, to be present in the breathing zone at levels that differ from the larger microenvironment of the room (Wallace, 2000). In this research, we consider the possibility that chemical interactions with occupant surfaces can influence breathing zone levels of harmful gas-phase species. Specifically, we will consider ozone and the reaction products that are generated by the reaction at skin, hair and clothing surfaces.

Ozone has been shown to be associated with mortality and morbidity, even at relatively low concentrations (Bell et al., 2006; National Research Council, 2008). Indoor concentrations of ozone are lower than outdoors, but integrated exposure and inhalation rates tend to be equally divided between indoor and outdoor environments (Weschler, 2006). These reduced levels are due to gas-phase (Weschler and Shields, 2000) and surface reactions (Morrison, 2008). Reaction products

include aldehydes, ketones, carboxylic acids, and secondary organic aerosols. The reaction products themselves are likely to be unhealthy, resulting in toxicants (e.g., formaldehyde), irritants and sensitizers. Several animal and human studies have identified eye and airway irritation (Wolkoff et al., 2000, 1999; Clausen et al., 2001; Wilkins et al., 2001; Tamás et al., 2006) as well as limited respiratory flow and possible long-term sensitization (Rohr et al., 2002) as the result of ozone-terpene reaction mixtures.

Personal exposure may also be influenced by ozone reactions with human skin oils and clothing. Ozone-human reactions have been shown to contribute to more than half of the total ozone loss in a densely occupied aircraft cabin (Tamas et al., 2006a,b). Pandrangi and Morrison (2008) estimate that a single occupant of a typical residential room will be responsible for approximately 10% of the total ozone removal. Measurements of the ozone-surface reaction probability with human hair (Pandrangi and Morrison, 2008) and clothing (Coleman et al., 2008) suggest that ozone uptake to the human surface is rapid and limited primarily by transport through the boundary layer surrounding the body. Thus, the ozone level within the boundary layer is predicted to be significantly depleted, potentially leading to low ozone levels in the breathing zone. This ozone concentration gradient was observed experimentally around human subjects by Liu et al. (1994). These reactions generate oxidation products specific to ozone oxidation of unsaturated compounds in human skin oils such as squalene and fatty acids. Products of note include nonanal, decanal, acetone, geranyl acetone, 6-methyl-5-hepten-2-one and dicarbonyls such as 4-oxopentanal (Coleman et al., 2008; Pandrangi and Morrison, 2008; Weschler et al., 2007). Dicarbonyl compounds are predicted to be particularly irritating and act as sensitizers (Anderson et al., 2007). To distinguish these reaction products from others generated in the gas-phase or at other surfaces, we designate the Ozone Reaction Products associated with the Human Surface (hair, skin and skin-oil coated clothing and accessories) as ORPHS. On a molar basis, at least 10–35% of the ozone that reacts will generate a volatile, inhalable, oxidation product (Coleman et al., 2008; Weschler et al., 2007). Thus, as ozone levels are depleted in the breathing zone, ORPHS will increase in the breathing zone. Gas-phase reactions that may occur between ozone and volatilized personal care products, coined 'near-head chemistry' (Corsi et al., 2007), are not considered in this research, but may further alter pollutant levels in the body's boundary layer.

Our goal was to estimate breathing zone concentrations of gases influenced by interactions with human integument. To achieve this goal, we experimentally validated computational fluid dynamics (CFD) models and used them for the calculation of ozone deposition on human surfaces. Using experimental measurements of ozone flux to the surface of a geometrically simplified human (a heated cylinder) we validated our CFD concentration boundary layer models. Then we applied the CFD analysis to analyze air flow and ozone reaction rate on surfaces of a manikin with a human geometry, positioned in a room with a ventilation system. The distribution of ozone and ORPHS concentrations in a room and in the air surrounding an occupant were simulated under a variety of ventilation rates and flow-patterns. Comparisons of breathing zone and room levels of ozone and ORPHS, allowed us to assess the relative importance of personal and room-level microenvironments for assessing exposure.

Methods

CFD modeling approach

Two room geometries were simulated. Geometry 1 represented an experimental chamber containing a heated cylinder, or 'human simulator,' with an ozone reactive surface. Chamber experiments (see Experimental Validation section) were used to validate the model and thereby avoid errors and uncertainties associated with the boundary conditions and numerical schemes that can occur with CFD modeling (Sørensen and Nielsen, 2003). This validated CFD model was then applied to geometry 2: a ventilated room containing a single occupant. This geometry was used to estimate the effect of the occupant thermal plume, and surface reactivity, on ozone and ORPHS concentrations in the breathing zone.

The Fluent 6.3 model was used to simulate steady-state, three-dimensional airflow and transport of ozone (FLUENT, 2006). The RNG k-ϵ turbulence model was applied to model the effect of turbulence, and was chosen based on previous studies (Chen, 1995; Posner et al., 2003) showing that this model provides better accuracy when applied to indoor airflow modeling than other two-equation models. Three-dimensional convection–diffusion equations for ozone transport were used to simulate the distribution of ozone:

$$\nabla \cdot \left(\rho \vec{u}\, C\right) = \nabla \cdot (\Gamma \nabla C) + S_{\mathrm{C}}, \quad \Gamma = \rho D_{\mathrm{ozone}} + \frac{\mu_{\mathrm{t}}}{Sc_{\mathrm{t}}} \tag{1}$$

where, ρ is air density, $\vec{u}$ is air velocity vector, C is mixing ratio of ozone, Γ is total diffusive flux of ozone, S_{C} is source or sink of ozone, D_{ozone} is molecular diffusion coefficient for ozone, μ_{t} is turbulent viscosity, and S_{C_t} is turbulent Schmidt number.

Since the computational model for the velocity field and mass transfer in the surface boundary layer depends on the size of the computation grid in the vicinity of a surface, a grid sensitivity analysis was

conducted to validate grid selection (See Grid sensitivity analysis section).

Ozone mixing ratio. The ozone mixing ratio in the supply air of the simulation was set to 30 ppb (ozone source). Based on mass transport to reactive occupant surfaces (ozone sink), the distribution of ozone in the room was simulated for a range of ventilation rates. The mixing ratio in the: (1) microenvironment of the occupant (breathing zone), (2) larger microenvironment of the room (bulk flow region), and (3) exhaust air were calculated based on weighted-average values of mixing ratios in relevant regions of the room.

Ozone boundary condition at occupant and human simulator surfaces. Because of the reactivity of ozone with occupant skin or clothes, the ozone concentration or mixing ratio (ppb) adjacent to human surfaces is likely to be very low and flux will be mass-transport limited (Pandrangi and Morrison, 2008). Thus, we set the ozone concentration equal to zero at the surfaces of the human simulator (geometry 1) and the occupant (geometry 2). This assumption has several advantages in simplifying the simulation, but also is consistent with measurements of surface reactivity. Reaction probabilities for skin oils on hair (Pandrangi and Morrison, 2008) and on soiled clothing (Coleman et al., 2008) were in the range of 10^{-4} or greater. For human-relevant mass-transport rates, Pandrangi and Morrison (2008) predicted that the ozone flux at a human surface approaches mass-transfer, rather than surface reaction rate, limits. The assumption of zero-concentration condition at the human surface simulates this mass-transfer limited system. The implications of a non-zero ozone concentration adjacent to these surfaces is considered in Appendix A.

ORPHS mixing ratio. The mixing ratio of ORPHS is calculated based on ozone depletion. In the simulation, ozone reacts only with the human surface, and the ORPHS generation rate is proportional to the ozone loss rate through the molar yield, Y (Weschler et al., 2007; Coleman et al., 2008; Pandrangi and Morrison, 2008). We assume that there are no other sources or sinks of ORPHS. For example, if the breathing zone mixing ratio is 20 ppb lower than the inlet (air supply) mixing ratio, then the ORPHS mixing ratio is (20 ppb)*Y. Formally, the mixing ratio of ORPHS at grid cell i, $C_{\mathrm{ORPHS},i}$ is given by,

$$C_{\mathrm{ORPHS,i}} = Y(C_{\mathrm{s}} - C_{\mathrm{i}}) \qquad (2)$$

where Y is the molar yield of one or multiple ORPHS, C_{s} is the supply diffuser mixing ratio of ozone and C_i is the ozone mixing ratio at a grid cell, i. Equation (2) implicitly assumes that the diffusivities of ORPHS are equal to ozone.

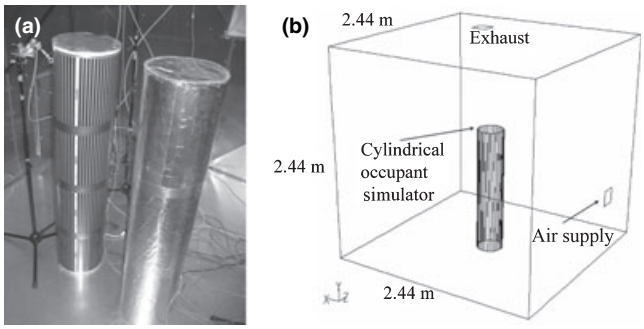

Fig. 1 CFD boundary conditions validation. (a) Heated cylinders used in ozone mass transfer tests (the left-hand cylinder was covered with a $NaNO_2$-coated fabric sheath and the right-hand cylinder was used for convective/radiative heat flux calculation). (b) Experimental chamber and CFD model geometry used in validation tests

Geometry 1

Figure 1a shows the cylindrical human simulators in the environmental chamber used in validation experiments. Figure 1b shows the experimental and room geometry used to determine the ozone concentration in the presence of a heated cylindrical human simulator. Ventilation rate in these validation experiments ranged from 0.70 to 0.90 air changes per hour in the chamber (see Experimental validation). This small ventilation airflow rate enabled buoyancy-driven flow from the cylinder to dominate in the space, providing non-uniform temperature and concentration fields around the cylinder. These conditions provided a challenging test case for the validation of overall ozone mass transport through the surface boundary layer.

Grid sensitivity analysis. To examine the dependency of mass transport on the grid size in the boundary layer, a CFD sensitivity analysis was conducted. Three different grid resolutions were analyzed. Surface adjacent grid cells with thicknesses 1, 3, and 10 mm and an aspect ratio of 1.5 were used. For each grid resolution in the boundary layer, the CFD results were compared and validated with airflow velocity and mass transfer coefficients measured experimentally.

Geometry 2

The validated CFD model was applied to simulate a more detailed, and realistic, geometry of a standing occupant in a room (Figure 2). The convective portion of the heat flux from the occupant was set to 30 W over a total occupant surface area of 1.8 m^2, which corresponds to a 1.73 m tall, 70 kg person (DuBois and DuBois, 1916). The surface convective heat flux was calculated for a standing occupant with 60 to 40% ratios between radiative and convective portion of the total heat flux (ASHRAE Handbook - Fundamentals,

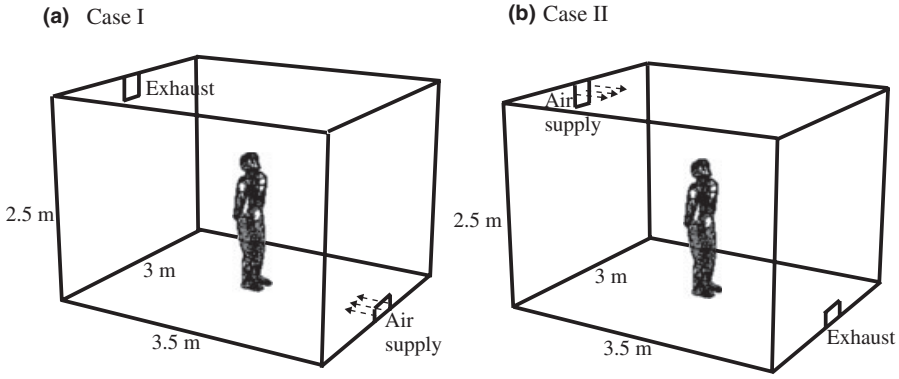

Fig. 2 Simulation geometry for ozone uptake experiments: (a) CASE I with the air supply opening at floor level in front of the occupant; (b) CASE II with the air supply at ceiling level behind the occupant

chapter 29, 2001). The occupant was centered in a room with dimensions of $3.0 \times 3.5 \times 2.5$ m, and the airflow in the room was supplied and exhausted in two different ways (CASE I and CASE II in Figure 2).

For each simulation case we analyzed the airflow distribution and the temperature field as well as the ozone concentration in the breathing zone. The breathing zone concentration was calculated as the volume-averaged concentration over a 500 cm^3 air volume below the nose tip. The effect of respiration on flow was not taken into account. Instead, we assume that the inhaled air is derived primarily from the rising thermal plume. This is consistent with findings that (1) the thickness of the plume at nose level reaches up to 0.015 m in front of the body (Gao and Niu, 2005), and (2) the inhaled concentration can be measured with sufficient accuracy ($< 5\%$) without breathing simulation if the sampling location is $<$ 0.01 m from the upper lip (Melikov and Kaczmarczyk, 2007).

Figure 2 shows the simulated occupant in the chamber for both cases. For each case, ozone concentrations in the breathing zone and bulk flow region were calculated for seven different ventilation rates: 0.5, 1, 2, 3, 5, 8.8, and 17.6/h. Ventilation rates lower than 5/h are typical of spaces in residential and commercial buildings (Waring and Siegel, 2008), while those higher than 5/h are associated with indoor environments such as automobiles (Park et al., 1998), operation rooms, or rooms with open windows on a windy day.

Based on the resulting breathing zone concentration, bulk air concentration, and the concentrations at supply inlet and exhaust, we calculated three parameters:

(1) *Ozone decay rate constant*, k_{ozone}. The ozone decay rate constant can be compared against typical air exchange rates, measured ozone decay rates (e.g., Lee et al., 1999) in buildings, and those predicted for occupants (Pandrangi and Morrison, 2008). The decay rate is defined as the difference between supply mixing ratio, C_s, and exhaust air mixing ratio, C_{ex}, multiplied by the air exchange rate, $\lambda = Q/V$ and normalized by C_{ex}.

$$k_{\text{ozone}} = \frac{\lambda(C_s - C_{ex})}{C_{ex}}. \tag{3}$$

(2) *Ozone ratio*, r_{ozone}. The ozone ratio relates the breathing zone mixing ratio to that of the larger microenvironment surrounding the occupant. An ozone ratio less than unity suggests that bulk-air ozone measurements will overestimate inhalation exposure or intake. This parameter is defined as the ratio between the breathing zone, C_{bz}, and bulk air, C_b, ozone mixing ratios. The bulk air mixing ratio was defined as the surface averaged value for a cylinder with 1 m radius and with the occupant in the center.

$$r_{\text{ozone}} = \frac{C_{bz}}{C_b}. \tag{4}$$

(3) *ORPHS ratio*, r_{ORPHS}. The ORPHS ratio relates the breathing zone mixing ratio to that of the microenvironment surrounding the occupant. An ORPHS ratio greater than unity indicates that bulk room measurements would underestimate inhalation exposure or intake of ORPHS. This parameter is defined as the ratio of the breathing zone ORPHS, $C_{\text{ORPHS,bz}}$, to the bulk-air ORPHS, $C_{\text{ORPHS,b}}$, mixing ratios. Note that the molar yield, Y, of ORPHS is eliminated in the ratio.

$$r_{\text{ORPHS}} = \frac{C_{\text{ORPHS,bz}}}{C_{\text{ORPHS,b}}} = \frac{(C_s - C_{bz})}{(C_s - C_b)}. \tag{5}$$

These three parameters were analyzed in conjunction with airflow distribution around the occupant, ventilation rate, and air mixing intensity.

Experimental validation

For CFD validation, four sets of experiments were conducted and replicated in the chamber depicted in

Figure 1a. The environmental chamber is a sealed and insulated stainless steel-clad room with a volume, V, equal to 13.8 m^3 and dimensions 2.4 m × 2.4 m × 2.4 m. The ventilation system is adjustable and the air exchange rate was set to approximately 0.8/h for all experiments. Experiments included measurements of air exchange rate, ozone removal rate, and temperature and velocity field in an environmental chamber. Ozone removal rate was measured at two locations, 0.15 m above the cylinder and at the exhaust. Surface temperature was measured at four positions, equally spaced vertically along the cylinder surface and at the center point of each wall. The air temperature was measured at the supply, the exhaust and the center of the chamber, as well as 0.025 m from the surface of the cylinder. An anemometer (HT-400, Sensor Electronic) was used to measure the air speed in the boundary layer of the thermal plume (0.025 m from surface of the cylinder). The human simulator was a heated cylinder with a surface area, A_{hs}, equal to 1.5 m^2 (height 1.5 m and diameter 0.3 m). The simple geometry of the cylinder enabled us to measure precisely the convective heat flux and the mass transfer coefficient at its surfaces while providing similar convective heat/mass transfer as an occupant (Topp et al., 2002). The removal rate of ozone in the whole chamber was analyzed for total heat fluxes of 30 and 60 W across the cylinder surface (20 W and 40 W/m^2 respectively) to test the CFD mass transfer models within a typical range of surface thermal boundary conditions. For both heat fluxes, ozone decay experiments were performed with and without an ozone reactive cotton sleeve fitted to the cylinder (see following section). For each experimental combination of heat flux and presence of cotton sleeve, the measurements were performed at least three times. In each experiment, air exchange rate and ozone decay rate in the chamber were simultaneously measured.

Ozone reactive sleeve for cylinder. To simulate transport limited uptake of ozone on an occupant, a snug-fitting sleeve was made to fit over the cylinder. This sleeve, made of cotton material similar to 't-shirt' cloth, was soaked in 500 ml of the following solution: 700 ml of water, 300 ml of methanol, 80 g of KNO_2, 20 g of Na_2CO_3, and 10 g of glycol. It was then hung to dry in low-ozone environment (sealed chamber) for 1 day. Filter material coated with this solution and dried has been shown to consume ozone at boundary layer transport limited rates (Morrison et al., 2003).

Quantification of convective and radiative heat transfer. The only heat source in the experimental chamber was the heated cylinder (Figure 1a). To examine the effect of heat flux on the mass transport of ozone, total heat fluxes of 60 and 30 W were applied across the cylinder surface. Since only the convective portion of the total heat flux affects the airflow in the boundary layer and the mass transfer of ozone, we quantified the convective and radiative portion of the total heat flux. Pure convective heat transfer was assumed for the aluminum foil covered cylinder (emissivity ≈0.1, Touloukian et al., 1972). Convective heat transfer from the cotton cylinder was calculated by applying a convection correlation (Novoselac et al., 2006) to the cotton-covered cylinder along with measurements of the temperature difference between cylinder surfaces and air. Subtracting the convective heat flux from the measured total heat flux, the radiative heat flux for the cotton-covered cylinder was obtained ($Q_{radiative} = Q_{total} - Q_{convective}$). This measurement was double-checked by solving the system of equations describing convective and radiative heat exchange between surfaces for the two cylinders (Modest, 2003). The calculated convective heat flux for the cotton-covered cylinder was used later in the CFD models as Neumann thermal boundary conditions.

Measurement of air exchange and ozone decay rates. The air exchange rate was measured by direct flow measurement and by tracer decay. An air flow station (GTx116-Pc, Ebtron) was used to measure the supply flow rate with an accuracy of ±3%. Carbon dioxide (CO_2) was used as an inert tracer gas to determine the chamber air exchange rate. Approximately, 10 l of pure CO_2 was released into the chamber through one of the injection ports located transversely opposite the supply inlet. Samples of air in the room were analyzed every 30 s thereafter using a non-dispersive, infrared CO_2 analyzer (Model LI-6252, LI-COR). The air exchange rate was assessed by the best fit to exponential decay of CO_2 verses time (ASTM E741, 2000), correcting for background CO_2. The agreement between the decay measurement and the measured flow at the inlet indicated minimal infiltration.

Total chamber ozone decay rates were used to determine ozone removal rates on the human simulator and on the chamber walls. Using an ozone generator supplied with pure oxygen, ozone was injected into the chamber until a well-mixed ozone mixing ratio of 150 ppb was achieved. Ozone injection was then discontinued and allowed to decay while ozone samples were collected at 1 min intervals. Ozone was measured using an ozone monitor (Model 205, 2B Technology) with a precision of 1 ppb. Ozone decay rate was quantified by a best fit to exponential decay. The difference between the ozone decay rate and air exchange rate was defined as the ozone decay rate associated with surface consumption (Niu et al., 2001). These experiments were repeated with and without the presence of the human simulator. The difference between the decay rate with, and without, the simulator is defined as the human simulator-specific ozone

decay rate, $k_{ozone,sim}$. The ozone deposition velocity, v_d, associated with the human simulator is

$$v_d = \frac{V}{A_{hs}} k_{ozone,sim}. \quad (6)$$

Results and discussion

CFD validation

Shown in Table 1 are the experimental results for the heated cylinder covered with the ozone reactive sleeve. The average velocity at the monitoring point located at 2.5 cm from the cylinder surface was 0.12 and 0.14 m/s for heat fluxes of 30 and 60 W, respectively. The thickness of the ozone concentration boundary layer was almost the same for both test cases because the velocity field around the cylinder for 20 and 40 W/m^2 heat fluxes was approximately the same (Table 1). The ozone concentration boundary layer thickness was in the range of 0.03–0.06 m, with smaller thickness in the lower part of the cylinder. For 20 W/m^2 total heat flux, the average cylinder surface temperature was 27.5°C and the average air temperature was 24.8°C; the calculated convective portion was 12 W. For a total heat flux of 40 W/m^2, the cylinder temperature was 30.2°C and the air temperature was 25.9°C, resulting in a total convective heat flux of 22 W.

Table 1 shows that the ozone decay rate for the cylinder surface was 0.57/h for the 30 W experiments and 0.66/h for 60 W experiments. The measurement uncertainty from repeated experiments was $<20\%$. Pandrangi and Morrison (2008) predicted the ozone removal rate for an occupant, based on typical mass-transfer coefficients and reaction probabilities, to be 0.44/h, which is about 23% lower than that measured here for the case of 30 W. However, correcting for the geometry of the simulation and the resulting mass-transfer coefficient of the 30 W simulations, the Pandrangi and Morrison prediction would have been 0.52/h, only 8% lower than the mean of measurements.

Shown in Table 2 are the CFD results for geometry 1, the model geometry and boundary conditions that are identical to the experimental setup. Also shown are the results of the sensitivity analysis obtained with the three different grid sizes for the first cells adjacent to the cylinder surface. Comparison of deposition velocities for the cell size of 1, 3, and 10 mm suggests that the cell size distribution moderately affects the velocity and concentration profiles when Neumann thermal boundary conditions are used. Comparison of experimental data and CFD results (CFD vs. Experiments in Tables 2) indicates that the difference in measured and calculated mass transfer coefficients range from 15 to 38%, with the best results for cases with finer grid resolution in the boundary layer. These differences are moderately larger than the standard deviation of results obtained by experimental measurements (SD in Table 1). Possible reasons for the deviation from experiments include (1) a non-zero concentration of ozone on the cotton sleeve (assumption of perfect sink), which may result in a lower deposition velocity compared with CFD results, (2) inaccuracy in experimentally determined heat flux and air exchange rate, and (3) an imperfect turbulence model for the occupant's thermal plume. However, the validation results are sufficiently accurate to give insight into ozone mass transfer in vicinity of an occupant and in the space and quantify the ozone mixing ratio in the breathing zone compared with the room levels on a relative basis for different airflow patterns.

Table 2 Scaling analysis for size of the first cell adjacent to the cylinder surface

Power (W)	Size of the first adjacent cell (mm)	Average sampling velocity (m/s)	Ozone loss rate (μg/h)[a]	Internal concentration (μg/m^3)[b]	Mass transfer coefficient (m/h)[c]	Difference (CFD vs. experiments)
30	1	0.13	279	28.0	6.98	0.20
	3	0.10	298	27.2	7.67	0.32
	10	0.09	298	26.0	8.02	0.38
60	1	0.15	289	26.0	7.79	0.15
	3	0.17	301	24.6	8.56	0.26
	10	0.18	308	23.8	9.06	0.34

[a]Ozone loss rate = $Q(C_s - C_{ex})$ for a supply concentration equal to 60 μg/m^3 (or mixing ratio = 30 ppb).
[b]Bulk concentration = C_b.
[c]Deposition velocity = $Q(C_s - C_{ex})]/[(C_b \times A_{hs})]$.

Table 1 Experimental results for heated cylinder experiments

Power (W)	Average sampling velocity (m/s)	Ozone decay rate (1/h)	Air exchange rate (1/h)	Ozone removal rate (1/h)	Deposition velocity, v_d (m/h) (mass transfer coefficient)
30	0.13	1.51	0.76	0.70	7.11
	0.12	1.46	0.87	0.53	5.42
	0.10	1.40	0.83	0.52	5.30
	0.12	1.38	0.79	0.54	5.49
	Average 0.12			Average (s.d.) 0.57 ± 0.08	Average (s.d.) 5.83 ± 0.85
60	0.14	1.62	0.74	0.83	8.41
	0.16	1.38	0.74	0.59	5.97
	0.13	1.35	0.71	0.59	5.95
	Average 0.14			Average (SD) 0.66 ± 0.14	Average (s.d.) 6.78 ± 1.42 v_d (60 W)/v_d(30 W) = 1.16

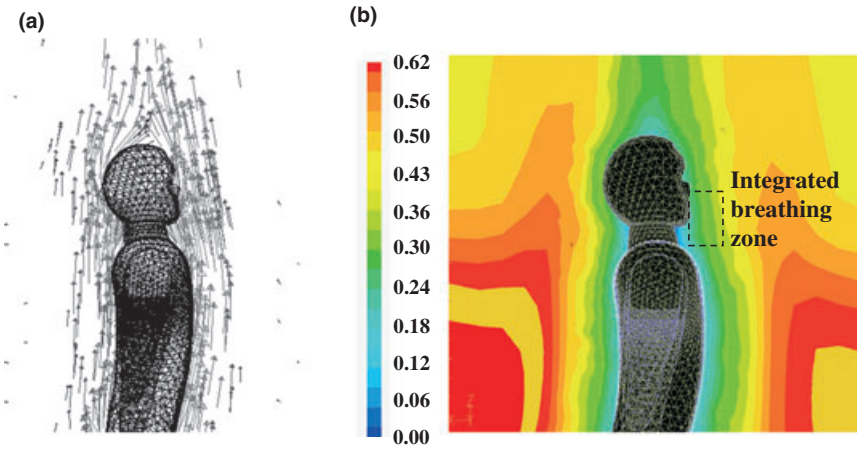

Fig. 3 (a) Occupant thermal plume for an air exchange rate equal to 0.5/h: mean velocity magnitude around the body = 0.1 m/s. (b) Contour of ozone concentration (normalized by chamber inlet concentration) around the body and sampling region for inhaled concentration

Exposure to ozone and ORPHS

The concentration gradient surrounding the simulated occupant is shown in Figure 3 for an air exchange rate of 0.5/h. The scale represents the concentration at that location normalized by the chamber inlet concentration. Within the frame, the highest ozone level is about 60% of the inlet value, but within 1 cm of the skin, the levels are approximately 20% of the inlet value. The thermal plume draws air up and across the reactive occupant surface, and the boundary layer consequently becomes depleted of ozone and conversely enriched with ORPHS (not shown in Figure 3). The breathing zone, as defined in this simulation, encompasses a region with ozone levels that are approximately one-third to one-half the level in the bulk air region (1 m from the body). Thus, the occupant is surrounded by a sheath, or personal cloud, of ozone-depleted, ORPHS enriched air.

To compare the results for different ventilation conditions, we provide in Figure 4 the calculated average air speed in the occupant surface boundary layer (4a), the ozone decay rate (4b), breathing zone ozone ratio (4c), and breathing zone ORPHS ratio (4d) as a function of air exchange rate, λ, for ceiling and floor inlet simulations. Figure 4a indicates that for air exchange rate, $\lambda < 5$/h, the air speed in the skin boundary layer changes little with an increase in λ. This result suggests that when $\lambda < 5$/h, the thermal plume dominates the airflow close to the occupant and that air movement in the room does not significantly disrupt the thermal plume. For $\lambda > 5$/h the air speed around the occupant increases significantly as λ increases for CASE I (floor supply), but changes little for CASE II (ceiling supply). This difference can be explained by examining Figure 5, which shows the velocity vectors for the highest analyzed λ (17.6/h). Figure 5a shows that the jet of air from the floor supply across the occupant's feet intensifies the velocity around the occupant surface, especially close to the legs of the occupant. Conversely, the jet from the ceiling supply circulates along the chamber surfaces including the ceiling and walls before approaching the occupant (Figure 5b). The circulated jet does not affect the airflow around the occupant as much as the direct floor supply jet, resulting in a smaller range of air speed close to the occupant than the floor supply. The average air speed in the chamber volume is nearly the same (0.01–0.04 m/s for $\lambda < 5$/h, 0.08–0.09 m/s for 8.8/h, and 0.18–0.19 m/s for 16.6/h) for both floor supply and ceiling supply over the studied air exchange rates. However, for $\lambda > 5$/h, the air speed close to the occupant surface strongly depends on the air supply pattern and this affects the exposure to ozone and reaction products.

The ozone decay rate is shown in Figure 4b. With the exception of the lowest λ, the decay rate increases consistently, but not strongly, as λ increases. The difference between floor and ceiling supply is slight for $\lambda < 5$/h, but the difference widens beyond this (Figure 4b). Comparison of Figure 4a and b suggests that an increase in the air speed in the surface boundary layer leads to an increase in the mass transfer rate, enhancing ozone deposition onto the surface. The difference between floor and ceiling supply is slight for $\lambda < 9$, but the difference widens beyond this. This difference can be explained by examining Figure 5, which shows the velocity vectors for the highest λ. As shown in Figure 5a, the jet of air from the floor supply across the occupant's feet counteract and destroys the convective plume. A fraction of the supply air hits the legs of the standing person and moves upwards by the thermal plume; the rest of the air circulates along the floor, wall, and ceiling and then moves downward near the head of the standing person. Figure 5b shows that the jet from the ceiling supply somewhat increases

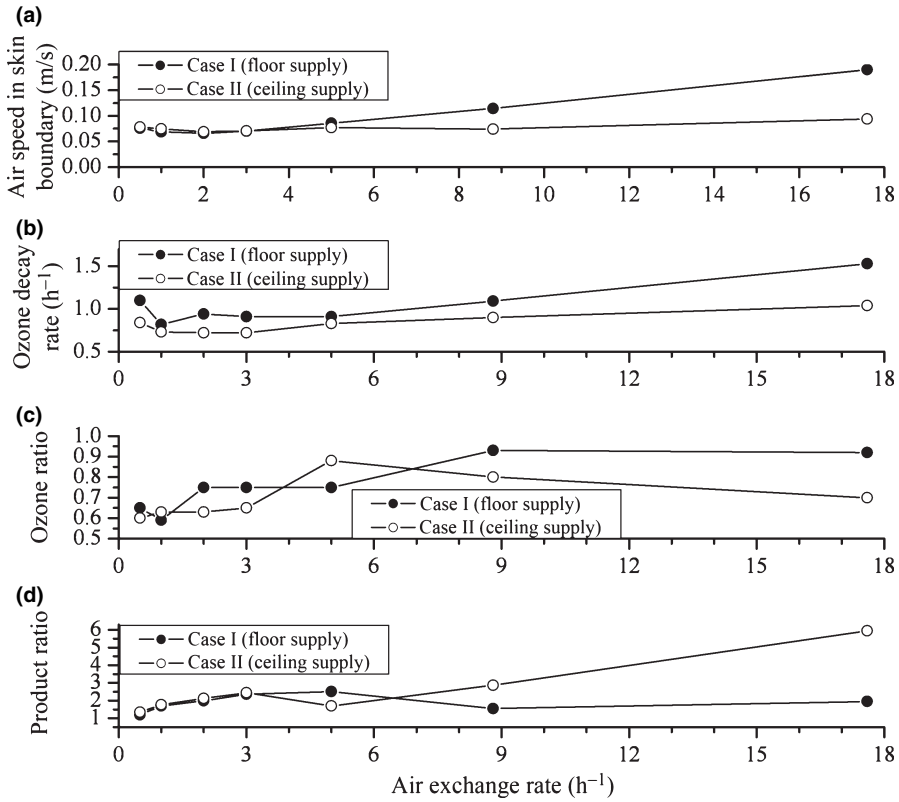

Fig. 4 Average air speed in the occupant surface boundary layer (a), ozone removal rate (b), ratio between inhaled concentration and average room concentration (c), and product concentration ratio (d) as a function of air exchange rate for the two characteristic airflow scenarios (CASEs): CASE I (floor supply) and CASE II (ceiling supply)

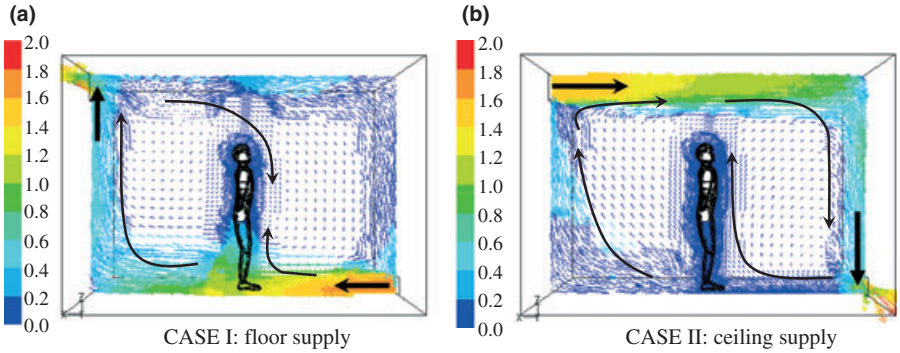

Fig. 5 Distribution of velocity magnitude and ozone concentration with air exchange rate of 17.6/h for the flow pattern: CASE I (floor supply) and CASE II (ceiling supply)

air flow upward across the occupant. Therefore, the two systems result in very different velocities in the boundary layer. The decay rate in this case is higher for CASE I, because the floor jet increases mixing intensity around the legs.

Over a wide range of air exchange rates, the ozone ratio, r_{ozone}, ranges from 0.6 to 0.9, indicating that the breathing concentration is 60–90% of the bulk air concentration (Figure 4c). For typical residential air exchange rates, up to 3/h, this ratio ranges from 0.6 to 0.8. Thus, ozone is depleted in the breathing zone and measurements of room levels will significantly over-estimate personal exposure or inhalation intake. As λ increases above 5/h, the ozone ratio increases with the floor supply (CASE I), but decreases with the ceiling supply (CASE II). Higher intensity air mixing occurs around the occupant in CASE I, flattening the concentration gradient between bulk air and the occupant surface. Further, boundary layer flow is directed downward, instead of upward, resulting in very little ozone removal (head region) before the air reaches the breathing zone. In CASE II, the air velocity and direction in the occupant boundary layer do not change substantially over a

large range of air exchange rates, the concentration gradient remains steep and the ozone ratio is much lower than for CASE II (0.7–0.8 compared with ~0.9 for CASE I over the same high air exchange rate region).

These results are in qualitative agreement with a study by Liu et al. (1994) which indicated that fixed-site indoor measurements may not represent personal exposure to ozone. They measured ozone mixing ratios in the boundary layer around seated volunteers using a continuous flow ozone analyzer. They found ozone ratios of 0.62–0.83 near the chest, 0.74–0.85 at the shoulder and ~0.83 below the nose. The orientation of the sample line significantly influenced the results, suggesting that sampling itself changed boundary layer flow. But these results are of the same order of magnitude as for this study and demonstrate that substantial reductions in inhalation intake may occur under typical indoor conditions. They also found that the personal exposure varies with micro-environmental conditions and occupant activity.

Enhancement in breathing zone levels of ORPHS is characterized by the product ratio, r_{ORPHS}, which is the ratio of the breathing zone levels and the levels in bulk air (Figure 4d). For values of $\lambda < 3$/h this ratio ranges from 1.5 to 2.5, meaning that product levels are roughly twice that in the rest of the room. Again, room measurements, for the reaction byproducts, will underestimate exposure substantially. There is an opposite tendency in the ozone ratio for floor and ceiling supplies and the trends do not consistently rise or fall with air exchange rate. The floor supply tends to have more air mixing around the occupant than the ceiling supply at very high λ, causing that concentration of reaction products in the breathing zone to approach bulk air levels. However, the airflow with the ceiling supply has the opposite effect for high λ, resulting in a large concentration difference between the breathing zone and bulk air. Because of the significant concentration gradient with ceiling supply, r_{ORPHS}, increases even more drastically for $\lambda > 5$/h. The product levels in the breathing zone do not decrease substantially as λ increases, even while air exchange effectively sweeps products out of the room. Since ozone levels are much higher outdoors, this finding suggests that breathing zone levels of ORPHS may be very high for individuals outside on a day with low velocity wind.

The results here cannot be directly extrapolated beyond this specific geometry. Sitting, standing, kneeling, reaching, turning, walking and other positions and motions will need to be assessed through modeling and measurement. However, higher velocities and air exchange rates may be a reasonable proxy for individual movement. Thus, the range of air velocities modeled around a single geometry provide an assessment of the probable range of ozone and ORPHS ratios anticipated in the breathing zone.

Conclusions

Personal exposure to ozone and reaction byproducts is influenced by ozone reactions with occupant surfaces including human skin oils and clothing. In this study, we show that in a typical indoor environment, the occupant thermal plume pulls air up and across the reactive occupant surface, and the occupant surface boundary layer consequently becomes depleted of ozone and conversely enriched with ORPHS. The extent of depletion/enrichment is large enough to make micro-environmental measurements suspect, especially when indoor exposures are thought to dominate total exposure (Weschler, 2006). Personal samplers that have been modified to reduce the impact of local gradients on ozone measurements (Liu et al., 1994) make measurements more consistent with the surrounding microenvironment rather than with the breathing zone. Are badge-style personal measurements of exposure relevant for intake, especially for the indoor fraction of exposure?

If ozone itself is the primary toxicant (National Research Council, 2008), morbidity/mortality correlations with outdoor levels may indicate that integrated outdoor exposure or peak ozone is more important than total exposure including indoor ozone exposure. Breathing zone levels when outdoors are probably close to outdoor site measurements. But low indoor ozone levels are lowered further in the breathing zone by reactions with the human surface. Therefore, indoor measurements would overestimate the indoor component of ozone intake and outdoor intake would dominate total intake.

If a byproduct of the ozone-human surface reaction is also an important toxicant (Weschler, 2006), then an appropriately weighted combination of ozone and its reaction products may be a better metric to compare against mortality. Under the present understanding of ORPHS generation mechanism, ORPHS levels in the breathing zone will follow outdoor ozone levels, barring indoor ozone sources. Even with lower indoor ozone levels, time-integrated ORPHS intake is much higher than outdoor intake. Therefore, indoor intake that follows outdoor ozone levels, could very well be realistically associated with observed adverse effects presently ascribed to ozone alone.

Acknowledgements

The research is partially supported by the National Science Foundation Integrative Graduate Education and Research Traineeship (IGERT) grant DCE-0549428, Indoor Environmental Science and Engineering, at The University of Texas at Austin. The Authors thank Brian Bell (Fluent Inc.) for help generating the detailed human geometry model used in this study.

References

Anderson, S.E., Wells, J.R., Fedorowicz, A., Butterworth, L.F., Meade, B.J. and Munson, A.E. (2007) Evaluation of the contact and respiratory sensitization potential of volatile organic compounds generated by simulated indoor air chemistry, *Toxicol. Sci.*, **97**, 355–363.

ASHRAE Handbook - Fundamentals, chapter 29. (2001) *American Society of Heating*, Atlanta, GA, Refrigerating and Air-Conditioning Engineers, Inc.

ASTM E741. (2000) *Standard Test Method for Detecting air Exchange in a Single Zone by Means of a Tracer gas Dilution*, Conshohocken, PA, American Society for Testing and Materials.

Bell, M., Peng, R.D. and Dominici, F. (2006) The exposure-response curve for ozone and risk of mortality and the adequacy of current ozone regulations, *Environ. Health Perspect.*, **114**, 532–536.

Cano-Ruiz, J.A., Kong, D., Balas, R.B. and Nazaroff, W.W. (1993) Removal of reactive gases at indoor surfaces: Combining mass transport and surface kinetics, *Atmos. Environ.*, **27a**, 2039–2050.

Chen, Q. (1995) Comparison of different k-ϵ models for indoor air flow computations. Numerical heat transfer. Part B, *Fundamentals*, **28**, 353–369.

Clausen, P., Wilkins, C.K., Wolkoff, P. and Nielsen, G.D. (2001) Chemical and biological evaluation of a reaction mixture of R-(+)-limonene/ozone - Formation of strong airway irritants, *Environ. Int.*, **26**, 511–522.

Coleman, B.K., Destaillats, H., Hodgson, A.T. and Nazaroff, W.W. (2008) Ozone consumption and volatile byproduct formation from surface reactions with aircraft cabin materials and clothing fabrics, *Atmos. Environ.*, **42**, 642–654.

Corsi, R.L., Siegel, J., Karamalegos, A., Simon, H. and Morrison, G.C. (2007) Personal reactive clouds: Introducing the concept of near-head chemistry, *Atmos. Environ.*, **41**, 3161–3165.

DuBois, D. and DuBois, E.F. (1916) A formula to estimate approximate surface area, if height and weight are known, *Arch. Intern. Med.*, **17**, 863–871.

FLUENT (2006) *Fluent 6.3 User*'s Guide Lebanon, NH, Fluent Inc.

Gao, N.P. and Niu, H.L. (2005) CFD study of the thermal environment around a human body: A review, *Indoor Built Environ.*, **14**, 5–16.

Klepeis, N.E., Nelson, W.C., Ott, W.R., Robinson, J.P., Tsang, A.M., Switzer, Paul., Behar, J.V., Hern, S.C. and Engelmann, W.H. (2001) The National Human Activity Pattern Survey (NHAPS): a resource for assessing exposure to environmental pollutants, *J. Expo. Anal. Environ. Epidemiol.*, **11**, 231–252.

Lee, K., Vallarino, J., Dumyahn, T., Ozkaynak, H. and Spengler, J. (1999) Ozone decay rates in residences, *Air Waste Manage. Assoc.*, **49**, 1238–1244.

Liu, L.J.S., Olson, M.P., Allen, G.A., Koutrakis, P., McDonnell, W.F. and Gerrity, T.R. (1994) Evaluation of the Harvard ozone passive sampler on human subjects indoors, *Environ. Sci. Technol.*, **28**, 915–923.

Melikov, A. and Kaczmarczyk, J. (2007) Influence of geometry of thermal manikins on concentration distribution and personal exposure, *Indoor Air*, **17**, 50–59.

Modest, M.F. (2003) *Radiative Heat Transfer*, San Diego, CA, Academic Press.

Morrison, G.C., Ping, Z., Wiseman, D.J., Ongwandee, M., Chang, H., Portman, J. and Regmi, S. (2003) Rapid measurement of indoor mass-transfer coefficients, *Atmos. Environ.*, **37**, 5611–5619.

Morrison, G.C. (2008) Interfacial chemistry in indoor environments, *Environ. Sci. Technol.*, **42**, 3495–3499.

National Research Council (2008) *Estimating Mortality Risk Reduction and Economic Benefits From Controlling Ozone Air Pollution*, Report by National Research Council, Committee on Estimating Mortality Risk Reduction Benefits from Decreasing Tropospheric Ozone Exposure. Washington, DC, The national Academic Press, ISBN-10: 0-309-11994-4.

Niu, J., Tung, T. and Burnett, J. (2001) Ozone emission rate testing and ranking method using environmental chamber, *Atmos. Environ.*, **35**, 2143–2151.

Novoselac, A., Burley, J.B. and Srebric, J. (2006) Development of New and Validation of Existing Convection Correlations for Rooms with Displacement Ventilation Systems, *Energy Buildings*, **38**, 163–173.

Pandrangi, L. and Morrison, G.C. (2008) Ozone interactions with human hair: Ozone uptake rates and product formation, *Atmos. Environ.*, **42**, 5079–5089.

Park, J.H., Spengler, J.D., Yoon, D.W., Dumyahn, T., Lee, K. and Ozkaynak, H. (1998) Measurement of air exchange rate of stationary vehicles and estimation of in-vehicle exposure, *J. Expo. Anal. Environ. Epidemiol.*, **8**, 65–78.

Posner, J.D., Buchanan, C.R. and Dunn-Rankin, D. (2003) Measurement and prediction of indoor air flow in a model room, *Energy Buildings*, **35**, 515–526.

Rohr, A., Wilkins, C.K., Clausen, P.A., Hammer, M., Nielsen, G.D., Wolkoff, P. and Spengler, J.D. (2002) Upper airway and pulmonary effects of oxidation products of (+)-alpha-pinene, d-limonene, and isoprene in BALB/c mice, *Inhal. Toxicol.*, **14**, 663–684.

Sørensen, D.N. and Nielsen, P.V. (2003) Quality control of computational fluid dynamics in indoor environments, *Indoor Air*, **13**, 2–17.

Tamas, G., Weschler, C.J., Bako-Biro, Z., Wyon, D.P. and Strom-Tejsen, P. (2006a) Factors affecting ozone removal rates in a simulated aircraft cabin environment, *Atmos. Environ.*, **40**, 6122–6133.

Tamas, G., Weschler, C.J., Toftum, J. and Fanger, P.O. (2006b) Influence of ozone-limonene reactions on perceived air quality, *Indoor Air*, **16**, 168–178.

Topp, C., Nielsen, P.V. and Sørensen, D.N. (2002) Application of Computer Simulated Persons in Indoor Environmental Modeling, *ASHRAE Trans.*, **108**, 1084–1089.

Touloukian, Y.S., DeWitt, D.P. and Hernicz, R.S. (1972) *Thermal Radiative Properties: Coatings*, New York, Plenum Publishing Corporation.

Wallace, L. (2000) Correlations of personal exposure to particles with outdoor air measurements: A review of recent studies, *Aerosol Sci. Technol.*, **32**, 15–25.

Waring, M. and Siegel, J. (2008) Particle loading rates for HVAC filters, heat exchangers, and ducts, *Indoor Air*, **18**, 209–224.

Weschler, C.J., Shields, H.C. and Naik, D.V. (1989) Indoor ozone exposures, *JAPCA: J. Air Waste Manage. Assoc.*, **39**, 1562–1568.

Weschler, C.J. (2006) Ozone's impact on public health: Contributions from indoor exposures to ozone and products of ozone-initiated chemistry, *Environ. Health Perspect.*, **114**, 1489–1496.

Weschler, C.J. and Shields, H.C. (2000) The influence of ventilation on reactions among indoor pollutants: modeling and experimental observations, *Indoor Air*, **10**, 92–100.

Weschler, C.J., Wisthaler, A., Cowlin, S., Tamas, G., Strom-Tejsen, P., Hodgson, A.T., Destaillats, H., Herrington, J., Zhang, J.J. and Nazaroff, W.W. (2007) Ozone-initiated chemistry in an occupied simulated aircraft cabin, *Environ. Sci. Technol.*, **41**, 6177–6184.

Wilkins, C.K., Clausen, P.A., Wolkoff, P., Larsen, S.T., Hammer, M., Larsen, K., Hansen, V. and Nielsen, G.D. (2001) Formation of strong airway irritants in mixtures of isoprene/ozone and isoprene/ozone/nitrogen dioxide, *Environ. Health Perspect.*, **109**, 937–941.

Wolkoff, P., Clausen, P.A., Wikins, C.K., Hougaard, K.S. and Nielsen, G.D. (1999) Formation of strong airway irritants in a model mixture of (+)-alpha-pinene/ozone, *Atmos. Environ.*, **33**, 693–698.

Wolkoff, P., Calusen, P.A., Wilkins, C.K. and Nielsen, G.D. (2000) Formation of strong airway irritants in terpene/

Appendix A. Influence of reaction probability on r_{ozone}

In the CFD analysis, section 'Ozone concentration vs. ozone reaction products associated with human surfaces,' the concentration of ozone at the body surface was set to zero to simulate flux limited only by ozone transport through the boundary layer. This may not always be the case for all types of clothing and Coleman et al. (2008) observed a reaction probability as low as 1.5×10^{-5} for clean clothes. Therefore, the impact of surface resistance on r_{ozone} and r_{ORPHS} are of interest.

Cano-Ruiz et al. (1993) showed that the overall resistance to mass transfer is given by,

$$\frac{1}{v_{\text{d}}} = \frac{1}{v_{\text{t}}} + \frac{4}{\langle v_{\text{b}} \rangle \gamma} \tag{A1}$$

where v_d is the overall mass-transfer coefficient or deposition velocity, v_t is the transport limited deposition velocity (m/h), $< v_{\text{b}} >$ is Boltzmann's velocity for ozone (1.3×10^6 m/h) and γ is the ozone-surface reaction probability.

The flux J to the body surface is given by,

$$J = v_{\text{d}} C_{\text{r,o}} = C_{\text{r,o}} \left(\frac{1}{v_{\text{t}}} + \frac{4}{\langle v_{\text{b}} \rangle \gamma} \right)^{-1} \tag{A2}$$

where $C_{\text{r,o}}$ is the reference concentration in the bulk air. Flux is also equal to,

$$J = v_{\text{t}} \left(C_{\text{r,o}} - C_{\text{f}} \right) \tag{A3}$$

where C_{f} is the ozone concentration in the air adjacent to the skin (film concentration). By symmetry in a dilute system, the relative ozone levels at steady-state will be the same regardless of the magnitude at any location. Mathematically, this is,

$$\frac{\left(C_{\text{r,o}} - C_{\text{i,1}} \right)}{\left(C_{\text{r,o}} - C_{\text{f,1}} \right)} = \frac{\left(C_{\text{r,o}} - C_{\text{i,2}} \right)}{\left(C_{\text{r,o}} - C_{\text{f,2}} \right)} \tag{A4}$$

where $C_{i,1}$ is the air concentration at location i for case 1 and $C_{i,2}$ is the concentration for location i, for case 2. For case 1, the transport limited case, $C_{\text{f},1} = 0$. For case 2, the reaction probability is $< < 1$ and $C_{\text{f,2}} > 0$.

Solving for A2–A4 for $C_{i,2}$ yields,

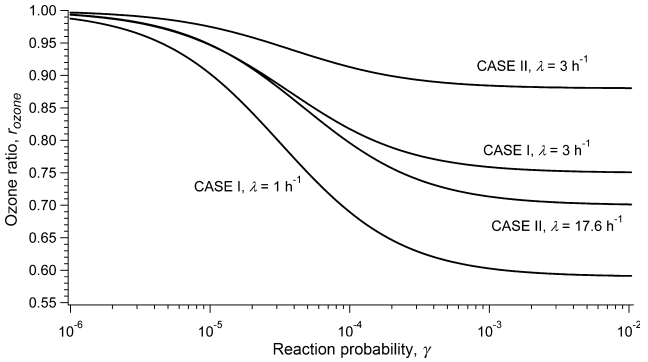

Fig. A1 Influence of the ozone reaction probability, γ, of the occupant surface (skin and clothing) on the ozone ratio, r_{ozone}

$$C_{\text{i,2}} = \left(\frac{4 v_{\text{t}}}{4 v_{\text{t}} + \langle v_{\text{b}} \rangle \gamma} \right) C_{\text{r,o}} + \left(\frac{\langle v_{\text{b}} \rangle \gamma}{4 v_{\text{t}} + \langle v_{\text{b}} \rangle \gamma} \right) C_{\text{i,1}}. \tag{A5}$$

Dividing through by the bulk air concentration, r_{ozone} for case 2 is given by,

$$r_{\text{ozone,2}} = \left(\frac{4 v_{\text{t}}}{4 v_{\text{t}} + \langle v_{\text{b}} \rangle \gamma} \right) + \left(\frac{\langle v_{\text{b}} \rangle \gamma}{4 v_{\text{t}} + \langle v_{\text{b}} \rangle \gamma} \right) r_{\text{ozone,1}}. \tag{A6}$$

Therefore, the results shown in Figure 4 can be adjusted for an area-averaged reaction probability. For an air exchange rate of 1/h using a floor air supply diffuser, v_t was 10.4 m/h. Combining this with a reaction probability to 5×10^{-5}, the breathing zone ozone ratio increases from 0.59 (no surface resistance) to 0.75. Shown in Figure A1 are curves representing the breathing zone ozone ratio for several conditions simulated.

The reaction probability does not strongly influence r_{ozone} for γ greater than 10^{-4}–10^{-3}. But below this, r_{ozone} increases substantially and below $\gamma = 10^{-6}$, r_{ozone} is nearly equal to 1. Therefore, an important question will be, 'How rapidly does clothing become soiled from wear and handling?' If a single touch of the hand imparts enough skin oils to cloth to increase its reaction probability to $> 10^{-4}$, then the low-end estimates of r_{ozone} are more relevant, even soon after dressing.